Compact and Broadband Adiabatically Bent Superlattice-Waveguides With Negligible Insertion Loss and Ultra-Low Crosstalk

Humaira Zafar, Bruna Paredes, Inas Taha, Juan E. Villegas, *Graduate Student Member, IEEE*, Mahmoud Rasras, and Mauro F. Pereira

***Abstract*—Broadband and ultra-low crosstalk integrated silicon superlattice waveguides are proposed and demonstrated, enabling high-density waveguide integration. The superlattice waveguides are implemented as S-shaped adiabatic bends that yield ultra-low crosstalks in the neighboring channels, and an extremely low insertion loss, for the TE polarization. Special materials or complex fabrication steps are not required. The bent superlattice waveguides are measured to have an average insertion loss $\leq$ 0.1 dB for all channels. The average crosstalk values are ≤ -37.8 dB and $\leq$ -45.2 dB, in the first nearest neighboring waveguide and the second nearest neighboring waveguide, respectively. The transmission spectra are measured over the wavelength ranges of (1.24 μm to 1.38 μm) and (1.45 μm to 1.65 μm), covering both communication wavelengths of 1310 and 1550 nm. The simulation results predict an efficient broadband performance over the 500 nm wavelength range (1200 nm to 1700 nm), covering all O, E, S, C, L & U bands. The proof of concept was done for a silicon-on-insulator platform and the approach is applicable to other waveguide geometries and integrated photonic platforms.**

***Index Terms*—Silicon Photonics, transverse electric, superlattices, optical waveguides, adiabatic, silicon-on-insulator.**

I. Introduction

SILICON photonics has made substantial progress in developing low-cost and large-scale photonic integration, further demanding low-loss and high-quality optical signal to meet the requirements for an ever-increasing number of channels [1]. High-density integration of photonic components demands low-energy high-bandwidth interconnects, flexible signal transmission, and negligible crosstalk to meet the stringent requirements of high-performance modern devices. To achieve high-performance, area-efficient, and large-bandwidth interconnects, an array of waveguides (superlattice waveguides) at a small pitch is a useful solution.

The bottleneck in future computer integrated circuits is waveguide interconnection as these systems require tens of thousands of waveguide channels. To increase the transmission capacity, different approaches have been developed such as arrayed waveguide grating [2], space division multiplexing [3], [4], adiabatic elimination procedure [5], optical phase array [6], [7], nanostrips between neighboring waveguides [8], metamaterials [9], and nanophotonics clocking [10]. Moreover, waveguide arrays have been developed on different platforms, such as, silicon nitride waveguides [11], InP waveguides [12], polymer waveguides [13], and SOI waveguides [14]. It is crucial to realize sharp bends and reduce the separation between the adjacent waveguides to obtain densely packed waveguide superlattice structures with small footprints. Silicon-on-insulator platforms exhibit high refractive index contrast and consequently allow sharp bending that significantly reduces the footprint.

Superlattice waveguides on SOI wafers have already been reported in [15], [16], [17], [18], [19], [20], introducing different approaches to reduce the crosstalk between neighboring channel. A phase mismatch is highly required between the modes of adjacent waveguides to suppress the crosstalk. In [16], a well-known asymmetric directional coupler theory has been utilized to obtain low crosstalk. The authors confirmed that the light in a large array of straight waveguides is not transporting to second, third and further nearest neighbors. This low crosstalk was obtained by realizing a phase mismatch between the modes propagating in the adjacent waveguides. The required phase mismatch was acquired by choosing the waveguides of different widths. To maximize the phase mismatch and minimize the crosstalk, the width difference between the adjacent waveguides must be as large as possible. But a high-order mode will be excited if the waveguides are too wide, and a large mode overlap between the neighboring waveguides will occur if the waveguides are too narrow. A similar superlattice design based on straight waveguides has been reported in [18], showing nearly ≈ -18 dB crosstalk over a 30 nm bandwidth for both orthogonal polarizations. In [16], the measured crosstalk is -20 dB over a 80 nm bandwidth. The cross-coupling and random fluctuations in the transmission were further studied as a function of the

Manuscript received 29 September 2022; revised 27 January 2023; accepted 30 January 2023. Date of publication 2 February 2023; date of current version 9 March 2023. The work of Humaira Zafar was supported by the Khalifa University of Science and Technology under Award FSU-2021-023. The work of Mauro F. Pereira was also supported by the Khalifa University of Science and Technology under Awards FSU-2021-023 and CIRA-2021-108. *(Corresponding author: Mauro F. Pereira.)*

Humaira Zafar and Mauro F. Pereira are with the Department of Physics, Khalifa University of Science and Technology, Abu Dhabi 127788, UAE (e-mail: humaira.zafar@ku.ac.ae; mauro.pereira@ku.ac.ae).

Bruna Paredes, Juan E. Villegas, and Mahmoud Rasras are with the Department of Electrical and Computer Engineering, New York University, Abu Dhabi 129188, UAE (e-mail: bp64@nyu.edu; jev1@nyu.edu; mr5098@nyu.edu).

Inas Taha is with the Department of Physics, United Arab Emirates University, Al Ain 15551, UAE (e-mail: inas_t@uaeu.ac.ae).

Color versions of one or more figures in this article are available at https://doi.org/10.1109/JSTQE.2023.3241617.

Digital Object Identifier 10.1109/JSTQE.2023.3241617

side-wall roughness in these superlattice waveguides by Yang et al. in [15]. Moreover, superlattice waveguides based on the bent structures have been reported in [17], [19]. To avoid excess crosstalk at the tight bends and enhance the phase mismatch, the same approach of different waveguide widths was used. In such designs, the crosstalk suppression is highly sensitive to the small variation in waveguide widths, requiring strict fabrication control. For instance, in [16], tighter control of the waveguide width and roughness is highly required to maintain low crosstalk (a 5 nm width variation can lead to an increase in crosstalk). Similarly, in [17], a width difference of 25 nm to 30 nm in the adjacent waveguides makes a considerable difference in crosstalk. Consequently, stringent fabrication control is needed because such width variations can usually occur by sidewall angles and roughness. However, these fabrication imperfections do not disturb the performance of our superlattice waveguides because we acquired a phase mismatch by changing the radius of the bent waveguide. In addition, a higher channel capacity cannot be achieved when phase mismatch is acquired with different waveguide widths. This issue was solved in [19], where the phase mismatch is acquired using a different bending radius and keeping the waveguide width constant. The bends chosen in these superlattices are constant-radius curves. The design with constant-radius bends has a drawback of high insertion loss (IL), due to light scattering (because of mode discontinuity) at the junctions where the curvature changes its sign. To avoid the losses mentioned above, the authors chose a minimum bending radius ≥ 5 μm. In [20], an enhanced optical field confinement was achieved by using a 10 μm period-sinusoidal silicon waveguide array with air as a top cladding. An air-cladding makes their design incompatible with most metal BEOL (back end of the line) processes, and 10 μm-period bent waveguide leads to a larger footprint. However, a radius of 1 μm to 2 μm is highly required to realize ultra-small footprint for the modern dense integrated circuits, with negligible junction losses. One way to get rid of this junction loss is to introduce a transversal offset between the two curves as mentioned in [21]. On the other hand, a more convenient approach is to use adiabatic transition at the tight junctions (radius of 1 μm to 2 μm), that leads to a gradual change in curvature [22], [23], [24], [25]. Such adiabatic transitions can be achieved by using adiabatic bends where the waveguide curvature linearly changes with the waveguide length. Along with achieving no junction losses in these adiabatic bends, the guided modes in the bent section can be gradually transformed with negligible mode distortion, and consequently, there is no intermodal crosstalk inside the same waveguide [26], [27], [28]. We use these bends, for the first time, to design dense superlattice waveguides with a minimum radius of 1.5 μm. These superlattice waveguides precisely eliminate the junction and radiation losses, and exhibit the following characteristics: 1) ultra-low IL, 2) negligible crosstalk, 3) broadband and 4) ultra-small footprint. Additionally, this design can be fabricated in current silicon foundries with the standard CMOS process. This is the first report of a high-density integration of curved silicon waveguides, showing negligible crosstalk, negligible transmission, and a compact footprint (with $R_{\min} = 1.5$ μm), over the 500 nm wavelength range (1200 nm to 1700 nm), covering all O, E, S, C, L & U bands. Our proposed waveguide superlattices exhibit the following characteristics:

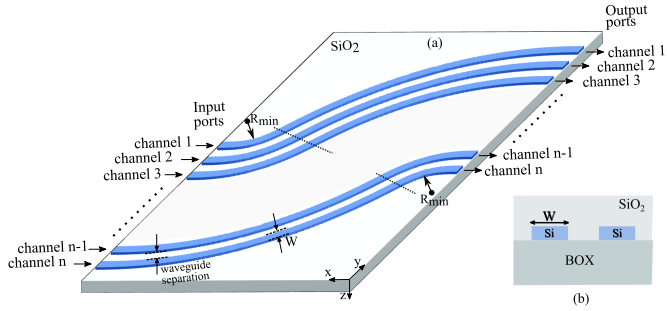

Fig. 1. Schematic illustration of the proposed n-channel superlattice waveguides, based on S-shaped adiabatic bends, with width $W = 500$ nm. The minimum radius of curvature is $R_{\min} = 1.5$ μm: (a) 3D view, (b) cross-sectional view.

- Broadband, over a 500 nm wavelength range (1200 nm to 1700 nm). The bandwidth of the previously reported superlattice waveguides is 80 nm.
- Extremely low TE IL, an average insertion loss ≤ 0.1 dB was measured for all channels, over the wavelength ranges of (1.24 μm to 1.38 μm) and (1.45 μm to 1.65 μm).
- The average crosstalk values are ≤ -37.8 dB and ≤ -45.3 dB, in the first nearest neighboring waveguide and the second nearest neighboring waveguide.
- Compact footprint with $R_{\min} = 1.5$ μm. Previously reported designs have $R_{\min} \geq 5$ μm.
- No stringent control of waveguide widths is required which makes it fabrication friendly.
- Compatible with the standard metal BEOL process.

II. Design and Simulation Results

The schematic of the proposed superlattice waveguides is shown in Fig. 1. These kinds of waveguides with no crosstalk are essential for high transmission capacity, compact and nanoscale silicon photonics integrated circuits. The basic principle of this proposed superlattice waveguides is based on the fact that the effective refractive index of the fundamental transverse electric (TE) mode in one waveguide is different from the effective refractive index of the fundamental TE mode in the adjacent waveguides (i.e. phase matching condition is not satisfied). An enhanced phase mismatch will lead to great crosstalk suppression which is necessary for high-performance dense integrated circuits. We present an array of curved waveguides and achieve a phase mismatch with a change in the radii of the neighboring waveguides. Moreover, The bends are adiabatic where the radius changes with the length of the curve. Consequently, we acquire a change in radius: 1) between two neighboring curves, and 2) along the path of each curve. Most importantly, waveguide bends tend to cause leakage of light that can lead to additional crosstalk, and can be more serious in dense superlattice waveguides. This leakage can be avoided with larger bending radii (≥ 5 μm) as reported in [17], [19]. However, small bending radii and reduced pitches are essential for many-channels multiplexer/demultiplexer applications to reduce the footprint. To overcome

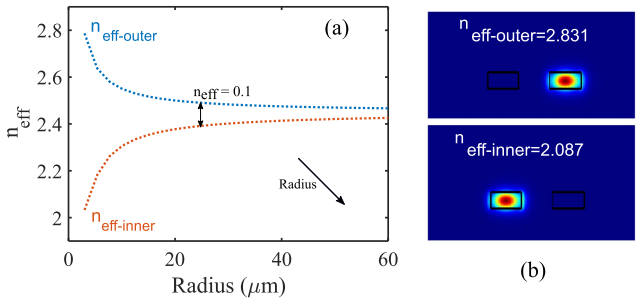

Fig. 2. (a) Calculated effective indices of $n_{eff-outer}$ and $n_{eff-inner}$ of both supermodes in a two-waveguide coupler, as a function of radius at a wavelength of 1550 nm. (b) Profiles of both super modes at Radius $= 3\,\mu$m .

this issue, we use adiabatic bends with a minimum radius of curvature $R_{\min} = 1.5\ \mu$m, indicating ultralow loss for the TE fundamental mode as reported in [22]. A schematic of the n-channel waveguide superlattice, with $R_{\min} = 1.5\ \mu$m is shown in Fig. 1(a). We simulate the S-shaped bends with a constant waveguide width of $W = 500$ nm, $R_{\min} = 1.5\ \mu$m, and waveguide separation of 600 nm (a 500 nm waveguide separation was chosen in fabrication), over the 500 nm wavelength range (1200 nm to 1700 nm), covering all O, E, S, C, L & U bands. The design is implemented on an SOI platform with a 2 μm-thick buried oxide (BOX) layer. The silicon layer is 220 nm-thick, and is surrounded by silicon dioxide as shown in the cross-section of Fig. 1(b). Such waveguides are single-mode, but with one weekly guided first-order TE mode present in the straight input section. This undesired first-order TE mode will radiate out of the waveguide, while propagating through the bent section, due to weak confinement. Consequently, only the fundamental TE mode will be present in the straight output section.

To calculate the phase mismatch for the fundamental TE mode, we choose two curved waveguides with a constant radius of Radius $= 3\,\mu$m, $W = 500$ nm and a waveguide separation of 500 nm, at a wavelength of 1550 nm. In this coupler, the crosstalk from one waveguide to another waveguide is explained by the following equation:

$$\frac{P_{1\to 2}}{P_1} = \frac{1}{\left(\frac{\Delta\beta}{2\kappa}\right)^2 + 1} \sin^2\left(L\sqrt{\left(\frac{\Delta\beta}{2}\right)^2 + \kappa^2}\right) \qquad (1)$$

Where $\Delta\beta$ is the difference in propagation constant or phase mismatch, κ is the coupling coefficient, and L is the propagation distance. Low crosstalk can be obtained if the phase mismatch is large ($\Delta\beta >> \kappa$). Such couplers lead to supermodes excitation which are shown in Fig. 2(b), illustrating two supermodes with effective indices of $n_{eff-outer}$ and $n_{eff-inner}$. The effective index values of both supermodes are plotted as a function of radius in Fig. 2(a). The effective index difference (phase mismatch) Δ_{neff} of both supermodes should be large enough (greater than 0.1 is standard practice) to achieve a weak coupling and low crosstalk. It is clear from Fig. 2(a) that a $\Delta_{neff} \geq 0.1$ is obtained for R$\leq 25\,\mu$m, indicating that the difference is quite high at smaller radii. Consequently, the selected adiabatic bends with $R_{\min} = 1.5\ \mu$m allow multiple channels, and further confirm:

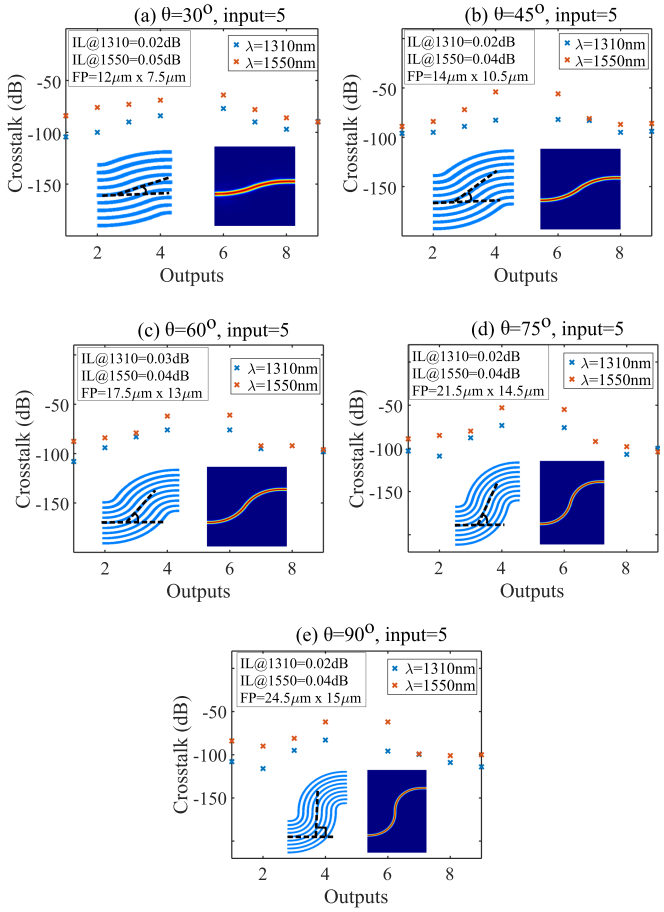

Fig. 3. Calculated values of insertion loss and crosstalk at two communication wavelengths of 1310 nm and 1550 nm, when light is launched at input 5. The curved waveguides are implemented as arcs of different angles with $R_{\min} = 1.5\ \mu$m. The top view of light propagation through port 5 is also shown, with bending angles of: (a) $\theta = 30°$, (b) $\theta = 45°$, (c) $\theta = 60°$, (d) $\theta = 75°$, (e) $\theta = 90°$. The footprints (FP) written on each panel show that the proposed superlattice structures are extremely area-efficient, fulfilling the requirements of the modern dense integrated circuits.

1) high phase mismatch, and 2) ultrasmall radiation loss due to sharp bending (no radiation and tight confinement of the modes in one individual waveguide can be seen in Fig. 2(b)).

The performance of the curved waveguide superlattices is studied with the 3D finite-difference time-domain method (FDTD) using the Lumerical package in our simulations [29], with refractive indices of 3.45 and 1.45 for the silicon and SiO_2, respectively (at a wavelength of 1550 nm). The crosstalk and the insertion loss are two important parameters (Fig. 3) that need to be calculated. IL is defined as the transmission through the input port. However, crosstalk is defined as the transmission through the neighboring ports, as explained by the following equations.

$$\text{Insertion Loss} = 10\ \log\ T_{nn} dB, \qquad (2)$$

$$\text{Crosstalk} = 10\ \log\ \frac{T_{nm}}{T_{nn}}\, dB, \qquad (3)$$

where T_{nn} is the transmission at the nth output port when light is launched into the nth input port. T_{nm} are the transmissions through the m ports (m=n±1, n±2, n±3,.....) when light is

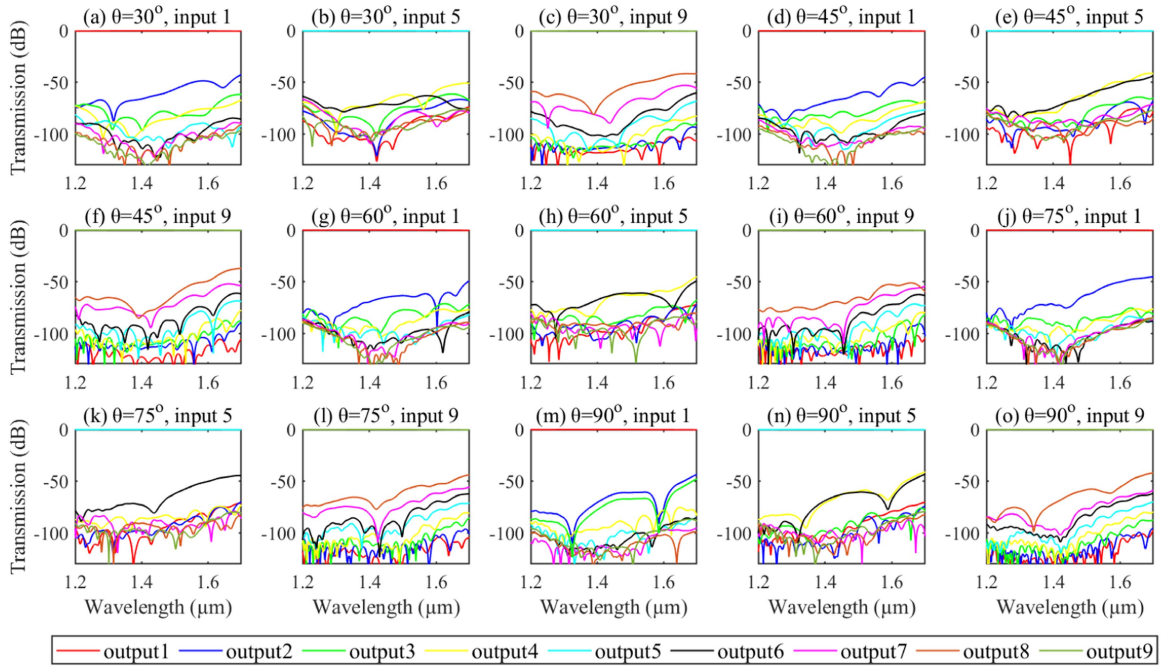

Fig. 4. Calculated transmission spectra for 9-channel waveguide superlattices for all bend angles of $\theta = 30°$, $45°$, $60°$, $75°$, and $90°$. Curves in each panel correspond to the transmissions at all output ports. The input port number at which the light is launched and the bending angles are written on the title of each panel. The color code for each output is given in the box above.

launched into the nth input port. For instance, when light is launched into port 5, T_{55} will be considered as IL. While the transmissions through all other neighboring ports, except port 5, will be taken as crosstalk. T_{nm} is an overlap integral [30] with the fundamental TE mode of the single waveguide. The average overlap loss is calculated to be ≤ 0.000166 (i.e., crosstalk $\leq -37.8\,\mathrm{dB}$). Coupling between the neighboring waveguides is the main source of the crosstalk and should be carefully calculated for high-performance systems.

A three-dimensional finite difference time domain (FDTD) simulations are carried out to calculate the IL and crosstalk when light is launched at input 5. Fig. 3 shows the crosstalk values at two communication wavelengths of $1310\,\mathrm{nm}$ and $1550\,\mathrm{nm}$. An array of bends was implemented as arcs of different angles, depicting in different panels of Fig. 3. The top view of light propagation through the middle waveguide (channel 5) is also shown in the inset of each panel. It is clear that the light is well confined in the middle waveguide and a negligible coupling is observed in the neighboring waveguides. It is further confirmed by the calculated crosstalk values, indicating extremely low values at both communication wavelengths for all angles of the curves. The worst-case calculated values of crosstalk at $1550\,\mathrm{nm}$ wavelength are $-64\,\mathrm{dB}$, $-54\,\mathrm{dB}$, $-61\,\mathrm{dB}$, $-53\,\mathrm{dB}$, and $-62\,\mathrm{dB}$ for the bending angles of $\theta = 30°$, $45°$, $60°$, $75°$, and $90°$, respectively. In addition, the footprints (FP) written on each panel show that the proposed superlattice structures are extremely area-efficient, fulfilling the requirements of the modern dense integrated circuits. Furthermore, IL values for all bending angles are less than $0.05\,\mathrm{dB}$ for both communication wavelengths, confirming that high-performance curved waveguide superlattices have been successfully implemented.

Having analyzed the IL and crosstalk values at two wavelengths, we now turn our attention over to calculating the spectral transmissions through all ports over a wavelength range of $1200\,\mathrm{nm}$ to $1700\,\mathrm{nm}$. We simulate 9-channel superlattice waveguides, and spectral transmissions are calculated at each output port after launching light at input ports 1, 5, and 9, for all bend angles, as shown in Fig. 4.

The curves in each panel of Fig. 4 correspond to the transmissions at all output ports. Fig. 4(a)–(c) illustrate the performance for $\theta = 30°$, with light launched at input ports $= 1$, 5, and 9, as written on the title of each panel. Similarly, the remaining panels depict the transmissions for all other bend angles with input light at the 1st, 5th, and 9th ports. It is clearly observed that the IL is negligible ($\leq 0.25\,\mathrm{dB}$) over a whole wavelength range of $1200\,\mathrm{nm}$ to $1700\,\mathrm{nm}$, and is negligible at both communication wavelengths. Additionally, an extremely low crosstalk value indicates that our obtained phase-mismatch leads to negligible coupling of light to the neighboring waveguides. As we achieve high-performance superlattice waveguides that work well in the bent sections, we can use multiple cascaded bends running through the entire chip. As our proposed superlattice waveguides perform equally well with all bend angles, the bend with $\theta = 30°$ will lead to a compact footprint fulfilling the requirements of the modern dense integrated circuits.

The device performance is further explained using 3D plots as shown in Fig. 5. The crosstalk transmission spectra are plotted at neighboring output ports when light is launched at each input port. The analysis is done for the same 9-channel superlattice with bends implemented with $\theta = 90°$. The IL and crosstalk curves are shown in Fig. 5(a) and (b), respectively. Fig. 5(b) depicts the crosstalk spectral transmissions through

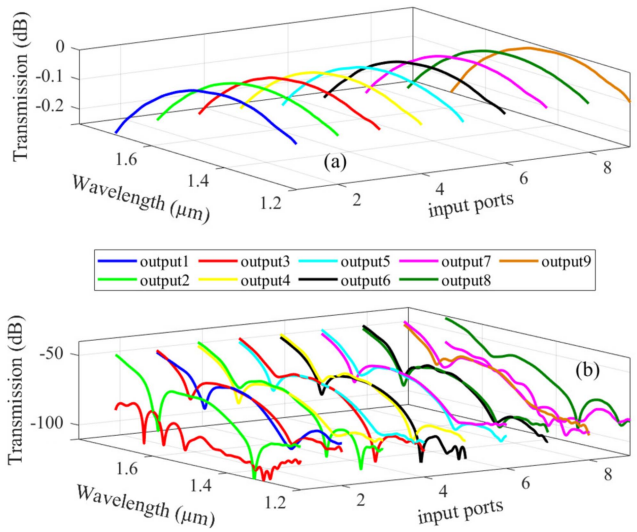

Fig. 5. Spectral transmissions for a 9-channel, and $\theta = 90^\circ$ waveguide superlattices, when light is launched at each input. (a) insertion loss (dB), (b) crosstalk (dB). The color code for each output is given in the box above.

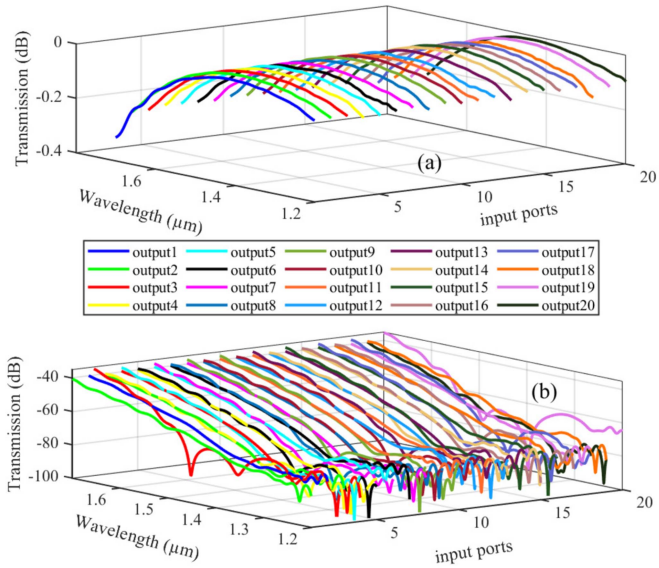

Fig. 6. Spectral transmissions for a 20-channel, $\theta = 45^\circ$ waveguide superlattices, when light is launched at each input. (a) insertion loss (dB), (b) crosstalk (dB). The color code for each output is given in the box above.

two neighboring ports at either side of the port with input light. It is clear from the spectral transmissions that an efficient and broadband performance has been acquired which is $\leq 0.25\,\mathrm{dB}$, and crosstalk is $\leq -50\,\mathrm{dB}$, over a $500\,\mathrm{nm}$ wavelength range.

The insertion loss and crosstalk are further investigated for more channels to check the performance and feasibility of the proposed design. Fig. 6(a) and (b) show the IL and crosstalk for a 20-channel superlattice waveguide, respectively. These bends are implemented as arcs of 45°. Again, a high performance and broadband performance has been exhibited which is $\leq 0.25\,\mathrm{dB}$, and crosstalk is $\leq -40\,\mathrm{dB}$, over a $500\,\mathrm{nm}$ wavelength range. An extremely low crosstalk is calculated which is below

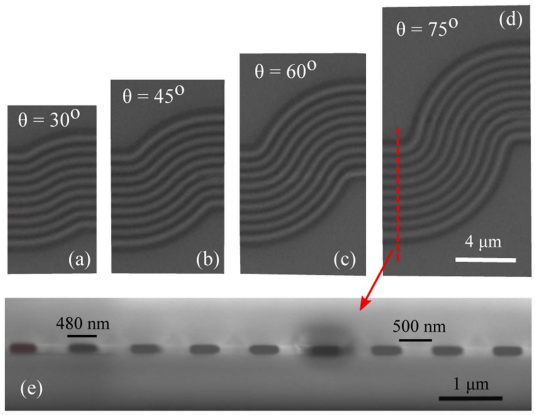

Fig. 7. (a-d) Optical images of the fabricated superlattice waveguides with angles $\theta = 30^\circ$, 45°, 60°, and 75°, (e) cross-sectional view (obtained using the focused ion beam method in scanning electron microscopy) at the position shown by the red dotted line.

$-74\,\mathrm{dB}$ and $-50\,\mathrm{dB}$ at the $1310\,\mathrm{nm}$ and $1550\,\mathrm{nm}$ wavelengths, respectively. Additionally, a negligible IL of $0.035\,\mathrm{dB}$ and $0.04\,\mathrm{dB}$ are computed, at $1310\,\mathrm{nm}$ and $1550\,\mathrm{nm}$ wavelengths, respectively.

III. Experimental Results

Several versions of the proposed superlattice waveguides were fabricated on a silicon-on-insulator platform with a $220\,\mathrm{nm}$-thick silicon layer and a $2\,\mu\mathrm{m}$-thick buffered oxide layer. The structures were patterned using electron beam lithography, and covered with a $2\,\mu\mathrm{m}$-thick oxide overcladding layer. The waveguides were fabricated with a constant width of $W = 500\,\mathrm{nm}$, $R_{\min} = 1.5\,\mu\mathrm{m}$, and waveguide separation of $500\,\mathrm{nm}$. Optical images (top view) for a 9-channel superlattice waveguides for the bend angles of ($\theta = 30^\circ$, 45°, 60°, and 75°, are shown in Fig. 7(a)-(d). Fig. 7(e) shows the cross-sectional view (obtained using the focused ion beam method in scanning electron microscopy (SEM)) at the position shown by the red dotted line. The top views using SEM images are not shown because the chip was covered with a $2\,\mu\mathrm{m}$-thick oxide layer. Two tunable lasers ($1.24\,\mu\mathrm{m}$ to $1.38\,\mu\mathrm{m}$) and ($1.45\,\mu\mathrm{m}$ to $1.65\,\mu\mathrm{m}$) were used as the light sources. The measured transmissions are shown in Fig. 8 and Table I. An electronic polarization controller was used to select the fundamental transverse electric mode. The light was edge coupled from a standard tapered lensed fiber into the chip, through input and output inverse taper-based spot size converters. The transmitted light was collected with a second lensed fiber and its power was measured using an InGaAs photodetector. To get a reliable measurement of the insertion loss, test structures with 16 cascaded devices were fabricated. It helps in minimizing the measurement errors caused by fiber misalignment and unreliability of the experimental setup. The transmission through the 16 cascaded devices was compared to the transmission through a reference straight waveguide to subtract the input/output coupling loss.

The measured transmission spectra are plotted in Fig. 8. The 3D plots show normalized transmission spectra for the 9-channel superlattice waveguides. Moreover, the measurements are done

TABLE I
SUMMARY OF THE PERFORMANCE OF THE FABRICATED SUPERLATTICE WAVEGUIDES WITH ALL ANGLES $\theta = 30°, 45°, 60°, 75°$, AND $90°$, INDICATING MINIMUM, MAXIMUM AND AVERAGE VALUES OF IL AND CROSSTALK WHEN THE LIGHT WAS LAUNCHED INTO CHANNEL 5, OVER THE WAVELENGTH RANGES OF (1.24 μM TO 1.38 μM) AND (1.45 μM TO 1.65 μM)

Angle		Wavelength = (1.24 μm to 1.38 μm) / (1.45 μm to 1.65 μm)				
		IL, channel 5	XT, channel 4	XT, channel 6	XT, channel 3	XT, channel 7
$\theta = 30°$	min	0.08/0.02	-36.7/-30.3	-32.6/-30.8	-43.1/-34.2	-38.2/-36.4
	max	0.17/0.07	-56.9/-49.8	-58.2/-53.2	-62.4/-56.2	-63.1/-57.4
	avg	0.08/0.03	-43.6/-37.8	-40.7/-40.1	-50.4/-45.7	-46.2/-45.5
$\theta = 45°$	min	0.08/0.04	-37.3/-33.1	-37.1/-32.1	-39.8/-35.4	-40.5/-36.4
	max	0.15/0.06	-54.9/-51.4	-58.9/-52.1	-57.1/-55.4	-60.8/-57.8
	avg	0.05/0.03	-43.9/-41.2	-44.8/-40.6	-47.9/-46.9	-47.2/-45.8
$\theta = 60°$	min	0.01/0.01	-35.4/-37.4	-33.3/-31.5	-38.1/-37.2	-38.8/-35.0
	max	0.1/0.09	-58.3/-54.4	-54.5/-51.8	-61.7/-59.4	-57.8/-55.7
	avg	0.1/0.06	-43.9/-41.3	-41.2/-39.6	-47.8/-45.3	-46.6/-45.3
$\theta = 75°$	min	0.05/0.01	-33.5/-32.8	-35.7/-30.01	-37.7/-37.0	-38.3/-38.7
	max	0.15/0.09	-56.5/-54.0	-55.9/-52.6	-59.7/-57.9	-59.8/-57.8
	avg	0.1/0.08	-44.3/-41.8	-42.8/-41.2	-48.1/-47.2	-46.9/-48.5
$\theta = 90°$	min	0.04/0.01	-36.1/-33.9	-34.6/-32.0	-39.1/-37.6	-37.5/-35.1
	max	0.12/0.07	-58.6/-54.2	-57.7/-51.4	-62.8/-57.9	-59.5/-57.8
	avg	0.1/0.06	-42.8/-41.2	-41.3/-38.8	-47.8/-45.2	-46.7/-45.7

for all angles ($\theta = 30°$, $45°$, $60°$, $75°$, and $90°$), over the wavelength ranges of (1.24 μm to 1.38 μm) and (1.45 μm to 1.65 μm). Fig. 8(a)–(e) depicts the performance of the superlattice waveguides for $\theta = 30°, 45°, 60°, 75°$, and $90°$, respectively. The left panels in each part of Fig. 8 correspond to the transmission spectra for (1.24 μm to 1.38 μm) wavelength range, and the right panels indicate the transmissions for (1.45 μm to 1.65 μm) wavelength range. The crosstalk was measured through two neighboring ports at either side of the port with input light. Each panel of Fig. 8 shows the normalized measured insertion loss through all 9 channels and normalized measured transmissions through two neighboring ports at both sides of the input port. It is clearly observed that the measured insertion loss is extremely small over both wavelength ranges. The bent superlattice waveguides are measured to have an average insertion loss ≤ 0.1 dB for all nine channels and five bend angles, over both wavelength ranges of (1.24 μm to 1.38 μm) and (1.45 μm to 1.65 μm). As the superlattice waveguides exhibit negligible IL, it is hard to quantify the exact losses with the manufactured devices, needing many more cascaded devices to obtain the exact IL measurement. It is evident from Fig. 10(e) and (f) that the transmission curves through the input waveguide and reference straight waveguide are overlapping. In this case, we end up with an error dominated by how well the fibers were aligned. In general, the obtained standard deviation of the measurements is kept low. For example, Fig. 9 plots the transmissions through the input ports (i.e. ILs) and standard deviation of loss for bend angle $\theta = 90°$, for both wavelength ranges. The blue curves in the top panels of Fig. 9 correspond to the ILs through all 9 channels, while the red curves plot the average. The bottom panels in Fig. 9 plot the standard deviation of loss, which is well below the error limits in a system.

The average crosstalk values are ≤ -37.8 dB and ≤ -45.3 dB for all bend angles, in the first nearest neighboring waveguide and the second nearest neighboring waveguide, respectively. The measurement of the input port and the neighboring ports was carried out independently. The power meters (Keysight N4477) were configured at a 10 dB range level (typical resolution of 600 nW) and -30 dB (typical resolution of 0.1 nW), to measure the power at the input port and cross ports, respectively. Each range level has a range of 50 dB, hence allowing for covering a long range when comparing the two measurements. The noise floor overall is then conditioned by the test setup. Also, typical standard deviations fall below 0.1 dB. Moreover, the simulated and measured IL and crosstalks are compared in Fig. 10. It shows the transmission spectra for a 9-channel superlattice waveguides for $\theta = 45°$. The crosstalk spectral transmissions are measured through two neighboring ports at either side of the input port number 5. IL is measured at the output of channel 5. Fig. 10(a) and (b) plots the simulated transmissions over a wavelength range of $1.24\,\mu$m to 1.38 μm and 1.45 μm to 1.65 μm, respectively. Fig. 10(b) and (c) depicts the normalized measured transmissions over a wavelength range of $1.24\,\mu$m to 1.38 μm and 1.45 μm to 1.65 μm, respectively. The transmissions through a simple straight waveguide and superlattice waveguides are shown in Fig. 10(e) and (f), where power at each output of the superlattice waveguides is not normalized. The reference waveguide is shown with a dotted line. It is clear that the transmissions through the reference waveguide and channel 5 are close to each other (see the blue curves) The measured spectral transmissions are close to the calculated values. The magnified views of the IL are also shown in Fig. 10, confirming a good agreement between the simulated and measured values. We attribute the differences between simulations and experiments to deviations in the slightly different widths during the fabrication process. Finally, Table I summarizes the performance of the fabricated superlattice waveguides with all angles $\theta = 30°$, $45°$, $60°$, $75°$, and $90°$. It indicates minimum, maximum and average

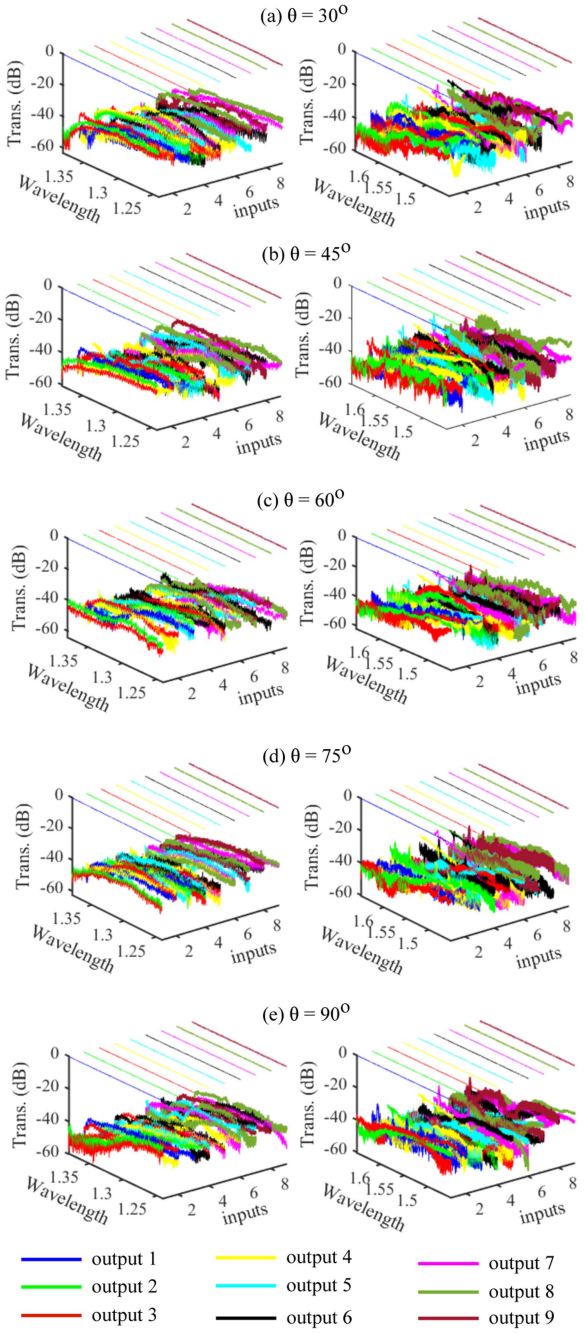

Fig. 8. Measured transmission spectra for 9-channel superlattice waveguides for all bend angles of $\theta = 30°, 45°, 60°, 75°$, and $90°$, with a constant waveguide width of $W = 500\,\text{nm}$, $R_{\min} = 1.5\ \mu\text{m}$, and waveguide separation of $500\,\text{nm}$. The left panels correspond to the transmission spectra for (1.24 μm to 1.38 μm) wavelength range, and the right panels indicate the transmissions for (1.45 μm to 1.65 μm) wavelength range. The crosstalk spectral transmissions are measured through two neighboring ports at either side of the input port.

values (resulting average of the full spectrum) of the insertion loss and crosstalk when the light was launched into channel 5, over the wavelength ranges of (1.24 μm to 1.38 μm) and (1.45 μm to 1.65 μm). The crosstalks in the third-nearest and further neighbors are extremely low and approaches the noise floor of our measurement setup.

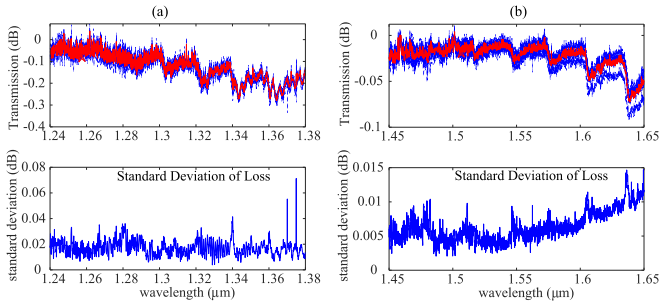

Fig. 9. The top panels depict the transmissions (i.e insertion loss) through all 9 channels (the 9 blue curves) with the average transmissions (the red curves), for $\theta = 90°$. The bottom panels plot the standard deviation of the insertion loss. (a) wavelength ranges of 1.24 μm to 1.38 μm and (b) wavelength range of 1.45 μm to 1.65 μm.

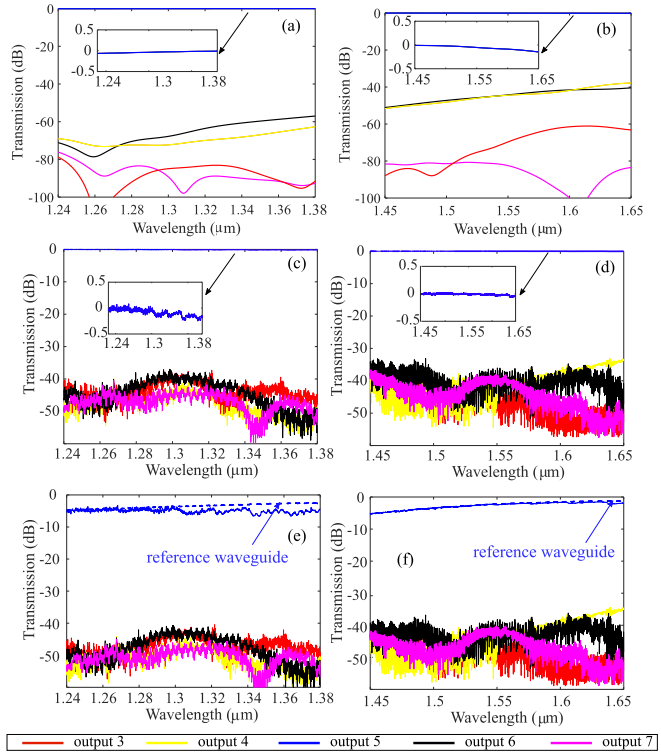

Fig. 10. Transmission spectra for a 9-channel superlattice waveguides for $\theta = 45°$, with a constant waveguide width of $W = 500\,\text{nm}$, $R_{\min} = 1.5\ \mu\text{m}$, and waveguide separation of $500\,\text{nm}$. The crosstalk spectral transmissions are measured through two neighboring ports at either side of the input port 5. (a), (b) simulated with wavelength ranges of 1.24 μm to 1.38 μm and 1.45 μm to 1.65 μm, (c, d) normalized measured power with wavelength ranges of 1.24 μm to 1.38 μm and 1.45 μm to 1.65 μm, (e, f) Power measured at the output of a simple straight waveguide (reference waveguide shown with a blue dotted line) along with the powers that are not normalized at each output port.

IV. Conclusion

This work presents novel superlattice waveguides on a silicon-on-insulator platform. The proposed design is implemented as an array of adiabatic bends, leading to a negligible TE transmission through the input channel and extremely low crosstalks in the neighboring channels. Measurements of the fabricated superlattice waveguides prove the feasibility of the proposed concept.

REFERENCES

[1] N. Margalit et al., "Perspective on the future of silicon photonics and electronics," *Appl. Phys. Lett.*, vol. 118, no. 22, 2021, Art. no. 220501.

[2] P. Cheben et al., "A high-resolution silicon-on-insulator arrayed waveguide grating microspectrometer with sub-micrometer aperture waveguides," *Opt. Exp.*, vol. 15, no. 5, pp. 2299–2306, 2007.

[3] E. Ip et al., "SDM transmission of real-time 10GbE traffic using commercial SFP transceivers over 0.5 km elliptical-core few-mode fiber," *Opt. Exp.*, vol. 23, no. 13, pp. 17120–17126, 2015.

[4] K. Chen et al., "Experimental demonstration of simultaneous mode and polarization-division multiplexing based on silicon densely packed waveguide array," *Opt. Lett.*, vol. 40, no. 20, pp. 4655–4658, 2015.

[5] M. Mrejen et al., "Adiabatic elimination-based coupling control in densely packed subwavelength waveguides," *Nature Commun.*, vol. 6, no. 1, pp. 1–7, 2015.

[6] D. Kwong, A. Hosseini, Y. Zhang, and R.T. Chen, "1× 12 Unequally spaced waveguide array for actively tuned optical phased array on a silicon nanomembrane," *Appl. Phys. Lett.*, vol. 99, no. 5, 2011, Art. no. 051104.

[7] L.-M. Leng et al., "Waveguide superlattice-based optical phased array," *Phys. Rev. Appl.*, vol. 15, no. 1, 2021, Art. no. 014019.

[8] Y. Bian et al., "Efficient cross-talk reduction of nanophotonic circuits enabled by fabrication friendly periodic silicon strip arrays," *Sci. Rep.*, vol. 7, no. 1, pp. 1–9, 2017.

[9] S. Jahani et al., "Controlling evanescent waves using silicon photonic all-dielectric metamaterials for dense integration," *Nature Commun.*, vol. 9, no. 1, pp. 1–9, 2018.

[10] B. Shen, R. Polson, and R. Menon, "Increasing the density of passive photonic-integrated circuits via nanophotonic cloaking," *Nature Commun.*, vol. 7, no. 1, pp. 1–9, 2016.

[11] Q. Han, M. Ménard, and W. Shi, "Superlattice arrayed waveguide grating in silicon nitride," *IEEE Photon. Technol. Lett.*, vol. 32, no. 22, pp. 1411–1414, Nov. 2020.

[12] P. Pan et al., "Flat-top AWG based on InP deep ridge waveguide," *Opt. Commun.*, vol. 355, pp. 376–381, 2015.

[13] B. Yang et al., "Compact arrayed waveguide grating devices based on small SU-8 strip waveguides," *J. Lightw. Technol.*, vol. 29, no. 13, pp. 2009–2014, 2011.

[14] Y. Onawa et al., "Polarisation insensitive wavelength de-multiplexer using arrayed waveguide grating and polarisation rotator/splitter," *Electron. Lett.*, vol. 55, no. 8, pp. 475–476, 2019.

[15] N. Yang et al., "Theory of high-density low-cross-talk waveguide superlattices," *Photon. Res.*, vol. 4, no. 6, pp. 233–239, 2016.

[16] W. Song et al., "High-density waveguide superlattices with low crosstalk," *Nature Commun.*, vol. 6, no. 1, pp. 1–9, 2015.

[17] R. Gatdula, S. Abbaslou, M. Lu, A. Stein, and W. Jiang, "Guiding light in bent waveguide superlattices with low crosstalk," *Optica*, vol. 6, no. 5, pp. 585–591, 2019.

[18] Y. Xie et al., "Ultra-dense dual-polarization waveguide superlattices on silicon," *Opt. Exp.*, vol. 28, no. 18, pp. 26774–26782, 2020.

[19] H. Xu and Y. Shi, "Ultra-broadband 16-channel mode division (de) multiplexer utilizing densely packed bent waveguide arrays," *Opt. Lett.*, vol. 41, no. 20, pp. 4815–4818, 2016.

[20] X. Yi, H. Zeng, S. Gao, and C. Qiu, "Design of an ultra-compact low-crosstalk sinusoidal silicon waveguide array for optical phased array," *Opt. Exp.*, vol. 28, no. 25, pp. 37505–37513, 2020.

[21] F. Ladouceur and E. Labeye, "A new general approach to optical waveguide path design," *J. Lightw. Technol.*, vol. 13, no. 3, pp. 481–492, Mar. 1995.

[22] H. Zafar et al., "Compact silicon TE-pass polarizer using adiabatically-bent fully-etched waveguides," *Opt. Exp.*, vol. 26, no. 24, pp. 31850–31860, 2018.

[23] H. Zafar et al., "Compact broadband (O, E, S, C, L & U. bands) silicon TE-pass polarizer based on ridge waveguide adiabatic S-bends," *Opt. Exp.*, vol. 30, no. 6, pp. 10087–100 95, 2022.

[24] H. Zafar et al., "High-extinction ratio polarization splitter based on an asymmetric directional coupler and on-chip polarizers on a silicon photonics platform," *Opt. Exp.*, vol. 28, no. 15, pp. 22899–22907, 2020.

[25] H. Zafar, M. F. Pereira, K. L. Kennedy, and D. H. Anjum, "Fabrication-tolerant and CMOS-compatible polarization splitter and rotator based on a compact bent-tapered directional coupler," *AIP Adv.*, vol. 10, no. 12, 2020, Art. no. 125214.

[26] D. Dai, J. Wang, and S. He, "Silicon multimode photonic integrated devices for on-chip mode-division-multiplexed optical interconnects (invited review)," *Prog. Electromagn. Res.*, vol. 143, pp. 773–819, 2013.

[27] T. Fujisawa, S. Makino, T. Sato, and K. Saitoh, "Low-loss, compact, and fabrication-tolerant Si-wire 90 waveguide bend using clothoid and normal curves for large scale photonic integrated circuits," *Opt. Exp.*, vol. 25, no. 8, pp. 9150–9159, 2017.

[28] M. Cherchi, S. Ylinen, M. Harjanne, M. Kapulainen, and T. Aalto, "Dramatic size reduction of waveguide bends on a micron-scale silicon photonic platform," *Opt. Exp.*, vol. 21, no. 15, pp. 17814–17823, 2013.

[29] Lumerical Inc. [Online]. Available: https://www.lumerical.com/products/

[30] G. Roelkens, D. Van Thourhout, and R. Baets, "High efficiency silicon-on-insulator grating coupler based on a poly-silicon overlay," *Opt. Exp.*, vol. 14, no. 24, pp. 11622–11630, 2006.

Humaira Zafar received the Ph.D. degree from the Masdar Institute, Khalifa University (KU), Abu Dhabi, UAE, in collaboration with the Massachusetts Institute of Technology, Cambridge, MA, USA. She is a Postdoctoral Fellow with Khalifa University. Her research interests include the development of novel photonic components for 6G networks and medical applications with KU. She is also involved in the development of high-speed, high-density, and low-power optical interconnects to replace traditional electrical interconnects. She has experience in the design, nanofabrication, and characterization of silicon photonic and optoelectronic devices. She is also involved in material characterization using SEM/EDX, TEM/EELS, FIB, and Lamella Preparation. Dr. Humaira contributed to several tapeouts with IME Singapore and GlobalFoundries, New York.

Bruna Paredes received the master's degree in electronics and telecommunications engineering from the University of Aveiro, Aveiro, Portugal, in 2014. She is currently a Research Engineer with the Electrical Department, New York University Abu Dhabi, Abu Dhabi, UAE. Her research interests include modeling, designing and testing optical devices within photonics integrated circuits for high-speed data communications.

Inas Taha received the Ph.D. degree in interdisciplinary engineering from Khalifa University (KU), Abu Dhabi, UAE. She is currently a Postdoctoral Fellow with the Physics Department, United Arab Emirates University (UAEU), Al Ain, UAE. She has more than seven years of experience in electron microscopy and cleanroom labs. Her work with UAEU focuses on the characterization of different phase change materials nanostructures for memory applications. Her research interests include the study of the interaction between GaN surface and H2O using a nanometer-scale GaN lamella structure with KU.

Juan E. Villegas (Graduate Student Member, IEEE) was born in Pereira, Colombia, in 1989. He received the B.E. degree in mechatronics from EIA University, Medellin, Colombia, in 2011, and the M.Sc. degree from Khalifa University, Abu Dhabi, UAE. in 2018. He is currently working toward the Ph.D. degree in electrical engineering with the Photonics Research Laboratory, Tandon School of Engineering, New York University, New York, NY, USA. Between 2011 and 2015, he was a Design Engineer and Researcher with the Marine Sciences and Technology Development Corporation, Cartagena, Colombia. Between 2015 and 2016, he was a Development Engineer with Bureau Veritas, Antwerp, Belgium, and a Research Engineer with Khalifa University between 2018 and 2019. His research interests include the design of integrated photonics systems in Silicon and Silicon Nitride for applications that include optical communications, hardware security, and quantum optics. Juan E. was the recipient of the 2018 Global Ph.D. Fellowship from NYU Abu Dhabi and 2016 Masdar Institute Fellowship. He is a Member of the IEEE Photonics Society, Optica, and Colombian Optical Society.

Mahmoud Rasras received the Ph.D. degree in physics from the Catholic University of Leuven, Leuven, Belgium. He is currently an Associate Professor of electrical engineering with New York University, Abu Dhabi, UAE. His research with IMEC focused on developing a spectroscopic photon-emission microscopy technique. He has more than 11 years of industrial research experience as a Member of the Technical Staff at Bell Labs, Alcatel-Lucent, NJ, USA. His research also include a wide range of activities focuses on the development of novel photonic components for next-generation optical and microwave photonic networks. His group with NYUAD developed a design for Photo-thermoelectric plasmonic enhanced graphene modulators and 2D-based photodetectors, all in silicon photonics platform. He was also a Former Director of the SRC/GF Center-for-Excellence on Integrated Photonics with Masdar Institute, Abu Dhabi, UAE. He is also a Member of the Mohammed bin Rashid Academy of Scientists.

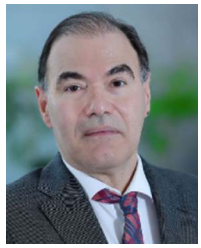

Mauro F. Pereira received the Ph.D. degree from the Optical Sciences Center, The University of Arizona, Tucson, AZ, USA, and has given important contributions to Nonequilibrium Greens Functions Many Body Theory of Transport and Optics of Semiconductor Materials. His research focuses on fundamental mathematical physics with applications to device development, with an impact in medicine and the environment, with a current emphasis on the protection of water critical infrastructures. He has been named SPIE Fellow in 2011 for his contributions to the Theory of Semiconductor Materials and Optics. He was the recipient of the SPIE Innovation awards in Quantum Sensing and Nano Electronics and Photonics (2019) for contributions to science and his service through organizing NATO TERA-MIR and COST. He was a Research Associate with CBPF, Uni-Rostock and TU-Berlin, Visiting Lecturer with Uni-Bremen, Senior Researcher with Tyndall Institute, Professor and Chair of theory of semiconductor materials and optics with Sheffield Hallam University, Sheffield, U.K., and the Head of the Department of Condensed Matter Theory, Institute of Physics, Academy of Sciences of Czech Republic, before joining Khalifa University, Abu Dhabi, UAE, as a Professor and the Chair of Physics Department.